Neutron scattering study of fluctuating and static spin correlations in the anisotropic spin glass Fe_2TiO_5

Yu Li [1,*], P. G. LaBarre [2], D. M. Pajerowski,[3] A. P. Ramirez [2], S. Rosenkranz [1], and D. Phelan[1]

[1]*Materials Science Division, Argonne National Laboratory, Lemont, Illinois 60439, USA*
[2]*Physics Department, University of California Santa Cruz (UCSC), Santa Cruz, California 95064, USA*
[3]*Neutron Scattering Division, Oak Ridge National Laboratory, Oak Ridge, Tennessee 37830, USA*

The anisotropic spin-glass transition, in which spin freezing is observed only along the c axis in pseudobrookite Fe_2TiO_5, has long been perplexing because the Fe^{3+} moments (d^5) are expected to be isotropic. Recently, neutron diffraction demonstrated that surfboard-shaped antiferromagnetic nanoregions coalesce above the glass transition temperature $T_g \approx 55$ K, and a model was proposed in which the freezing of the surfboard magnetization fluctuations leads to the anisotropic spin-glass state. Given this model, we have carried out high-resolution inelastic neutron scattering measurements of the spin-spin correlations to understand the temperature dependence of the intrasurfboard spin dynamics on neutron (picosecond) timescales. Here, we report on the temperature-dependence of the spin fluctuations measured from single-crystal Fe_2TiO_5. Strong quasi-elastic magnetic scattering, arising from intrasurfboard correlations, is observed well above T_g. The spin fluctuations possess a steep energy–wave vector relation and are indicative of strong exchange interactions, consistent with the large Curie-Weiss temperature. As the temperature approaches T_g from above, a shift in spectral weight from inelastic to elastic scattering is observed. At various temperatures between 4 and 300 K, a characteristic relaxation rate of the fluctuations is determined. Despite the freezing of most of the spin correlations, an inelastic contribution remains even at base temperature, signifying the presence of fluctuating intrasurfboard spin correlations to at least $T/T_g \approx 0.1$, consistent with an energy landscape that is a hybrid between conventional and geometrically frustrated spin glasses.

I. INTRODUCTION

Spin glasses [1] are systems in which magnetic moments freeze below T_g into configurations which can possess short-range order but also inherent randomness and lack long-range order. The formation of spin glasses is usually associated with a characteristic rugged landscape of metastable states resulting from the interplay of random disorder and frustration, the precise roles of which are still under significant debate [2–6]. Experimentally, the observed T_g of spin glasses depends upon the timescale of the experimental probe because the energies of the spin dynamics are strongly temperature dependent, particularly in the vicinity of T_g. Often, the frequency dependence of T_g, measured via AC magnetic susceptibility ($1–10^5$ Hz), is modeled either by a Vogel-Fulcher relation [7] or a dynamical scaling law [8]. Inelastic neutron scattering experiments, on the other hand, measure the Fourier reciprocate of a spin-spin correlation function on the much faster timescale of picoseconds ($\sim 10^{12}$ Hz). Additionally, unlike AC susceptibility, neutron scattering probes spin-spin correlations which give rise to peaks at specific wave vectors. Authors of previous reports of inelastic neutron scattering on conventional spin glasses such as Cu-Mn [9,10], Ni-Mn [11], and $Y(Mn_{0.9}Al_{0.1})_2$ [12] have indicated

that the temperature-dependent spin relaxation rates, extracted from the energy widths of the observed cross-section, can similarly be described by a Vogel-Fulcher law. Nevertheless, whereas Vogel-Fulcher predicts spin-spin correlation lifetimes to diverge at T_g, the observed behavior remains poorly understood. For instance, in some conventional systems such as Cu-Mn, this divergence does not occur, but rather temperature-independent relaxation rates were observed below T_g [9]. On the other hand, in some spin glasses which exhibit moderate frustration and are thus considered unconventional, such as in $Y_2Mo_2O_7$ [13], $CeNi_{0.4}Cu_{0.6}$ [14], $(Ni_{0.4}Mn_{0.6})TiO_3$ [15], and $BaFe_{2-x}Ni_xAs_2$ [16], only elastic signals were observed below T_g, consistent with completely frozen spins at the base temperature within the instrumental resolution. The study of spin glasses that exhibit unique or anomalous behavior may therefore lead to a more advanced understanding of the dynamics and spin-freezing processes.

In light of the different behaviors of conventional and strongly frustrated spin glasses, a particularly anomalous system is the pseudobrookite compound Fe_2TiO_5 which possesses an anisotropic spin-glass transition below $T_g \approx 55$ K; a cusp in susceptibility is seen only along the c axis, with no visible anomaly along a or b [17–23]. This is puzzling because Fe^{3+} is an isotropic s state (d^5) without single-ion anisotropy. Furthermore, the Fe^{3+} ions are randomly located on the A and B sites of the pseudobrookite structure, like A-B mixing in inverse spinels, which further reduces the

*yu.li@anl.gov

likelihood of, say, an interaction-induced anisotropy. Since the Weiss temperature $\theta_{CW} \simeq -900\,K$ indicates the presence of strong antiferromagnetic (AFM) interactions with significant frustration $f = \theta_{CW}/T_g \approx 16$, Fe_2TiO_5 is clearly in the class of strongly frustrated magnets. Our recent neutron diffraction study of the spin correlations in this system revealed the presence of strong diffuse scattering indicative of nanoscale order [24]. We found that strong geometrical frustration limits correlations along the *b* axis to nearest neighbors only. Furthermore, evidence of nanoscale surfboard-shaped regions was observed, with the surfboards developing at temperatures well above T_g. Within the surfboards, the magnetic moments are aligned parallel or antiparallel to the *a* axis (i.e., perpendicular to the direction where spin freezing is observed in susceptibility). The magnetic Fe^{3+} and nonmagnetic Ti^{4+} cations are understood to be randomly distributed on the two different crystallographic sites in Fe_2TiO_5. The nonmagnetic Ti^{4+} can thus be thought of as spin vacancies. The anisotropic spin freezing was then understood because of a fluctuation-induced intersurfboard interaction, i.e., a purely magnetic version of the van der Waals force [24].

While the formation of surfboards begins on cooling at $T > 5T_g$, it should be noted that this is not an example of a Griffith's phase since the AFM intrasurfboard order parameter is qualitatively different from the ensuing spin glass forming at T_g. Our previous neutron diffraction measurements [24], performed on Corelli [25], provided both elastic and total intensities, where the *elastic* intensity is measured within an $\approx 1-meV$ energy resolution, and the *total* represents the summation over both elastic and inelastic scattering contributions. This analysis hinted at the presence of varying static and dynamic spin correlations over a wide temperature range; however, to properly probe their static vs dynamic nature, true inelastic neutron scattering measurements are required. Only the results of limited inelastic measurements on Fe_2TiO_5, which were interpreted within the context of Vogel-Fulcher scaling, have been reported in the literature [22,23]. Given the much more recent observation of the surfboards, more comprehensive measurements are needed.

Here, we report on the results of inelastic neutron scattering measurements of a Fe_2TiO_5 single crystal at several temperatures above and below T_g. Spin fluctuations resulting in quasi-elastic magnetic neutron scattering are observed well above T_g. The quasi-elastic scattering shows a strongly anisotropic wave vector transfer (**Q**) dependence and is peaked at the positions in **Q** space where we previously reported evidence of surfboards in diffraction experiments. No change in the position of the wave vector of magnetic scattering is observed with increasing energy, indicating a very steep dispersion relation due to strong Fe-Fe exchange interactions. As the temperature is decreased toward T_g, a continuous slowing down of the fluctuations and a transfer of spectral weight from quasi-elastic to elastic scattering is observed, indicating spin freezing on the terahertz timescale. Nevertheless, quasi-elastic scattering remains observed down to $T/T_g \approx 0.1$, signifying a remnant presence of spin fluctuations [26], in contrast to a completely frozen spin scenario. In addition, fluctuations at heretofore unobserved wave vectors are also observed and are consistent with a slight canting of the

moments. Thus, Fe_2TiO_5 exhibits features at large **Q** and short times that are a hybrid of conventional and GF spin glass.

II. DETAILS OF EXPERIMENTS AND DATA ANALYSIS

The single crystal of Fe_2TiO_5 was grown by J. P. Remeika (deceased), formerly of Bell Labs, and comes from the same collection which we have previously characterized [24]. Inelastic neutron scattering measurements were performed on the Cold Neutron Chopper Spectrometer [27] at the Spallation Neutron Source, Oak Ridge National Laboratory. Empty can measurements were subtracted as a background. We used standard data reduction routines to transform data to physical coordinates with Mantid [28]. Experimentally, we define $\boldsymbol{Q} = \boldsymbol{k}_i - \boldsymbol{k}_f$ and $\hbar\omega = E_i - E_f$, where $\boldsymbol{k}_i$ and $\boldsymbol{k}_f$ are the incident and scattered wave vectors and E_i and E_f are the incident and scattered neutron energies. The sample has an orthorhombic lattice with *a*, *b*, and *c* of ∼3.73, 9.31, and 10.07 Å, respectively, and was aligned with *c* normal to the horizontal scattering plane, thus providing only limited detector coverage along *L*. Unless otherwise specified, the values of *L* throughout this paper are 0 by default. Measurements were performed with $E_i = 3.32\,meV$ or $E_i = 12\,meV$, and four-dimensional (**Q** and $\hbar\omega$) volumes of intensity were constructed from a series of rotations of the sample around the axis normal to the horizontal scattering plane. The data were symmetrized according to Laue symmetry *mmm*. The energy resolution at the elastic line was 0.1 and 0.7 meV full width at half maximum for $E_i = 3.32$ and 12 meV, respectively [29].

To separate the elastic and quasi-elastic (inelastic) contributions to the $\hbar\omega$ dependence of neutron scattering spectra appropriately, we consider that the measured intensity represents a convolution of the intrinsic scattering function $S(\boldsymbol{Q}, \hbar\omega)$ with a Gaussian resolution function $g(\hbar\omega, \Gamma_{res})$ of width Γ_{res}:

$$I(\boldsymbol{Q}, \hbar\omega) = \int_{-\Delta}^{\Delta} S(\boldsymbol{Q}, \hbar\omega) \times g(\hbar\omega - \hbar\omega', \Gamma_{res}) d(\hbar\omega').$$

Here, Δ is a cutoff energy much larger than Γ_{res}.

III. RESULTS AND DISCUSSION

In Fig. 1, we present the measured elastic ($\hbar\omega = 0$) neutron scattering patterns in the [*H*, *K*, 0] plane at $T = 1.5$, 55, 100, 200, and 300 K with $L = [-0.3, 0.3]$ reciprocal lattice units (r.l.u.) for $E_i = 12\,meV$ and $T = 1.5$, 100, 200, and 300 K with $L = [-0.2, 0.2]$ r.l.u. for $E_i = 3.32\,meV$. The intensities are integrated over an energy range comparable with or smaller than the instrumental resolution. Streaks of scattering that are narrow in *H* and extended in *K* are observed at $H = n + \frac{1}{2}$, $n = 0, \pm 1, \pm 2 \ldots \leqslant 100\,K$. This reflects the formation of surfboards as we described previously [24]. As we will discuss below, the scattering within this elastic window consists of a true elastic contribution (within the resolvable energy of the instrument) as well as the central part of a broadened quasi-elastic component, which is inherently inelastic. In addition to these sharp streaks, there are fainter and broader blobs of intensities centered at the same location in reciprocal space. These blobs lack a significant temperature dependence and indeed remain at higher temperatures
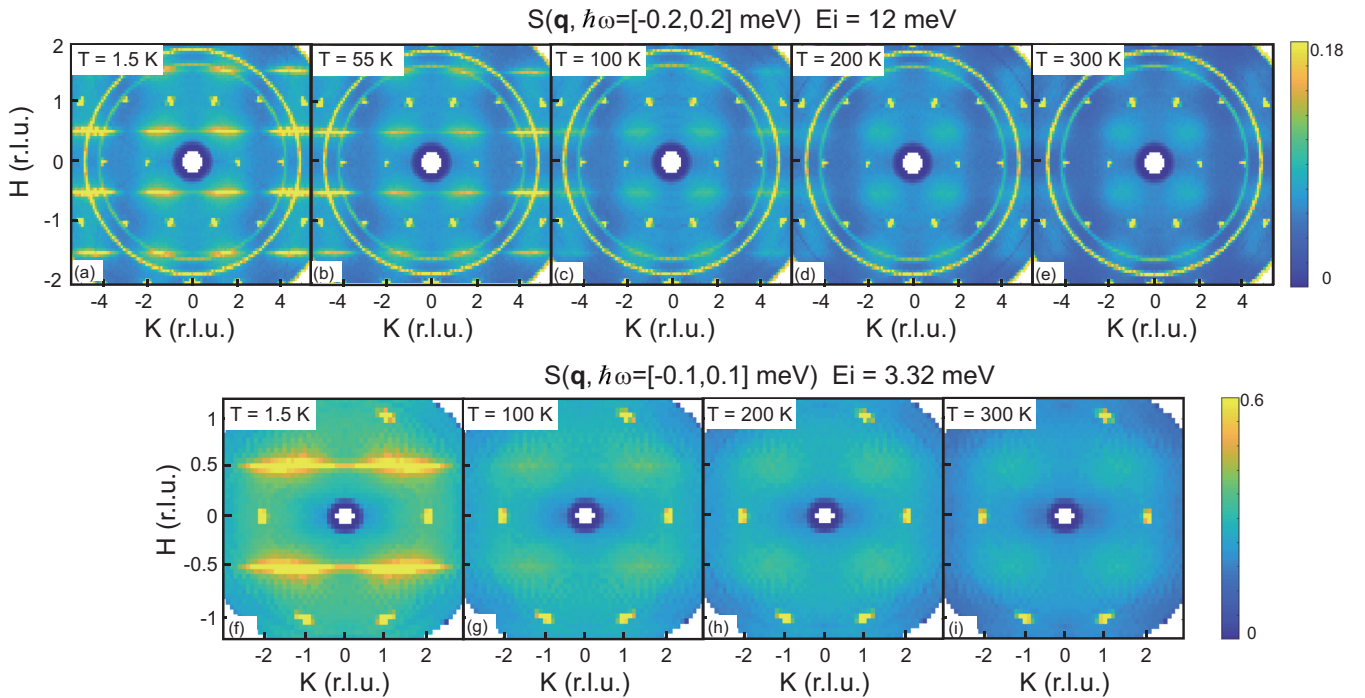
FIG. 1. Two-dimensional images of neutron diffraction intensities in the $HK0$ plane for different temperatures and incident neutron energies. Bright spots at integer numbers are nuclear Bragg peaks. Narrow streaks below 55 K at $H = n + 0.5, n = 0, \pm 1, \pm 2 \ldots$ are diffuse scattering associated with the surfboard nanoregion. There are broad temperature-independent intensities at the same location persisting up to 300 K, and they reflect the underlying structural disorders. (a)–(e) Neutron diffraction measured with $E_i = 12$ meV. (f)–(i) Neutron diffraction measured with $E_i = 3.32$ meV.

($T > 100$ K) [Figs. 1(c)–1(e), 1(h), and 1(i)], suggesting that they may be structural rather than magnetic in nature and likely arise from underlying structural disorder due to the site mixing of Fe^{3+} and Ti^{4+} cations.

Figure 2 shows inelastic neutron scattering intensity $S(\boldsymbol{Q}, \hbar\omega)$ in the $[H, K]$ plane at $L = 0$ at two characteristic $\hbar\omega$, 2 and 6 meV, for a series of temperatures. At both values of $\hbar\omega$, the shape of the intensity mimics the low-temperature elastic scattering pattern. This immediately indicates that the correlations being probed are intrasurfboard, as the nature of the correlation is implicated by its $\boldsymbol{Q}$ dependence. This inelastic scattering persists up to the highest measured temperature (300 K), demonstrating the existence of fluctuating intrasurfboard correlations far above T_g. These fluctuations are gradually enhanced upon cooling toward T_g. Below T_g, the intensities are dramatically suppressed due to spin freezing and transfer of the spectral weight into the elastic channel; however, there are remnant intensities, as shown in Figs. 2(a) and 2(f), indicating that there are remaining fluctuating intra-surfboard correlations at the lowest temperature we can reach. Furthermore, as seen in a color image of these residual spin fluctuations in Fig. 3(a), the steepness of these fluctuations as a function of H and $\hbar\omega$ is clearly seen. In Fig. 3(b), the momentum dependence of these spin fluctuations along H at a series of energies is presented. A Lorentzian fit does not exhibit any broadening of momentum linewidth as energy increases, indicating the existence of large local exchange coupling. We note here that no gap is observed at 1.5 K, consistent with the absence of either single-ion anisotropy or long-range order.

To gain further insight into the temperature dependence of the intrasurfboard spin dynamics, we present in Fig. 4 energy spectra at constant $\boldsymbol{Q} = (0.5, 1.5)$ at a series of temperatures where the spectra are dominated by the intensity arising from intrasurfboard correlations. We fit these energy-dependent spectra to the sum of a purely elastic component, given by a delta function scaled by an amplitude $f_0 \, \delta(\hbar\omega)$ and a quasielastic component, both of which are convolved with an instrumental resolution. The amplitude f_0 is proportional to the strength of the purely elastic component. For the quasi-elastic component, we consider that the scattering function corresponds to that of a damped zero-energy mode. The resulting $S(\hbar\omega)$ is given by

$$S(\hbar\omega) = f_0\delta(\hbar\omega) + \frac{\chi_0\Gamma\hbar\omega}{(\hbar\omega)^2 + \Gamma^2} \frac{1}{1 - \exp\left(\frac{-\hbar\omega}{k_B T}\right)}.$$

Here, Γ is a measure of the relaxation rate and is inversely proportional to the lifetime of the zero-energy mode, and χ_0 is a measure of the staggered susceptibility. The amplitude of the elastic contribution f_0 as function of temperature is shown in Fig. 3(b). As the temperature decreases all the way down to the base temperature, a substantial increase of the elastic contribution is clearly observed at T_g. The rapid increase in this contribution mirrors the increase of correlation length and indicates that the freezing of intrasurfboard correlations is strongly connected to the spin-glass transition, even though the latter is dominated by intersurfboard correlations. The slight increase of the intensity f_0 at 100 K and above may come from a background of elastic nuclear contribution. In
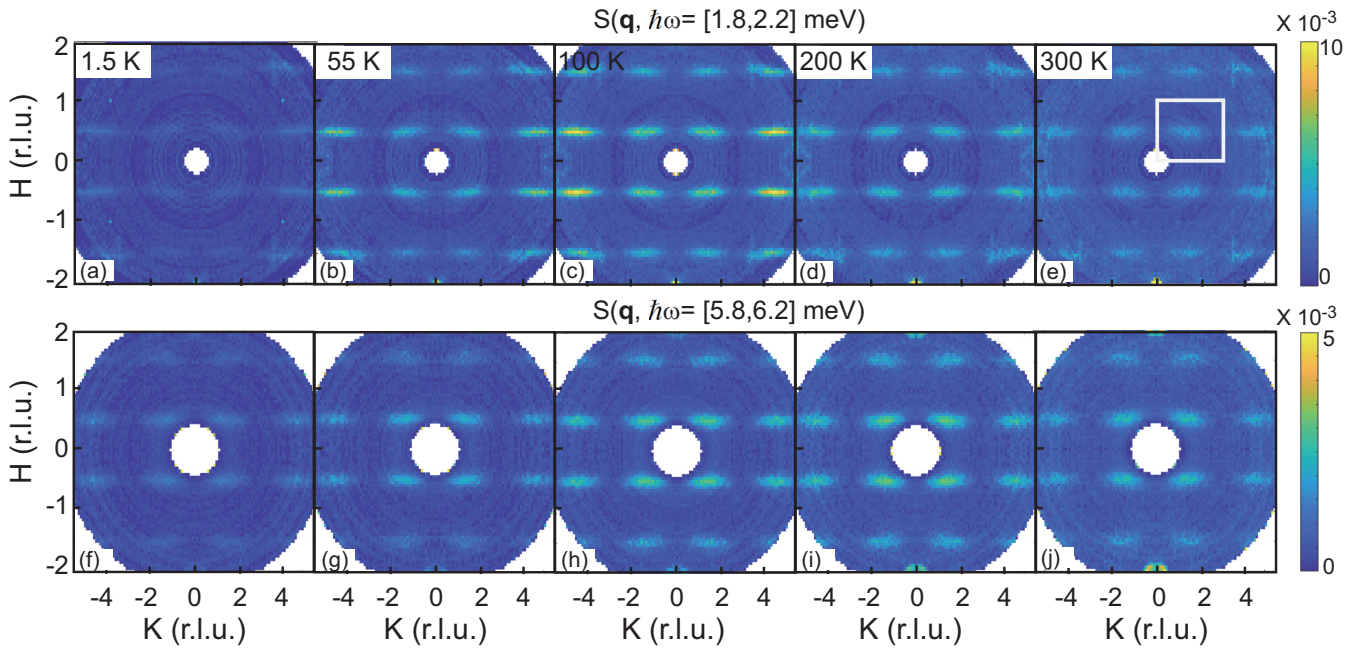
FIG. 2. Inelastic neutron scattering intensities plotted in the [H, K, 0] plane at different temperatures and energy transfer. Intensities arising at $(\pm 2, 0, 0)$ are acoustic phonons. (a)–(e) Spin fluctuations measured at $\hbar\omega = 2$ meV for five different temperatures. The white square in (e) represents an approximate periodicity of these spin fluctuations in the [H, K, 0] plane, as discussed in the text. (f)–(j) Spin fluctuations measured at $\hbar\omega = 6$ meV.

Fig. 4(c), the temperature dependence of Γ, which is obtained from the quasielastic contribution, is shown. A reduction of Γ on cooling, estimated from the measurement with $E_i = 12$ meV, starts to happen well above T_g, from 4.6 meV at 300 K to 2.3 meV at 55 K, like other spin glasses, and is interpreted as a characteristic of spin freezing. However, due to the limited points above T_g, we cannot determine whether the Vogel-Fulcher scaling rule is violated or not. We note that the value of Γ at low temperatures is still finite and significantly larger than the instrumental resolution, suggesting existence of dynamics below T_g. The staggered susceptibility

$\chi_0(\boldsymbol{Q})$ with $\boldsymbol{Q} = (0.5, 1.5, 0)$ displayed in Fig. 4(d) shows a maximum at T_g, indicating enhanced AFM correlations on approaching T_g.

In Figs. 5(a)–5(d), we show the scattering intensities in the [H, K, 0] plane at an energy transfer $\hbar\omega = 0.5 \pm 0.2$ meV measured with $E_i = 3.32$ meV at different tempera-
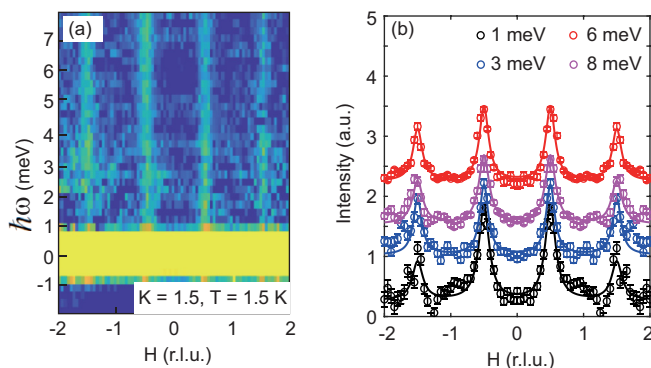

FIG. 3. (a) Color image plot of inelastic neutron scattering intensities as a function of H and energy at 2 K. Vertical dispersionless fluctuations are clearly observed at half integer H. (b) Cuts along the [H, 1.5, 0] direction at various energies at 1.5 K. There is a constant shift for each scan along the y axis. Solid lines are fitting results with a Lorentzian function.
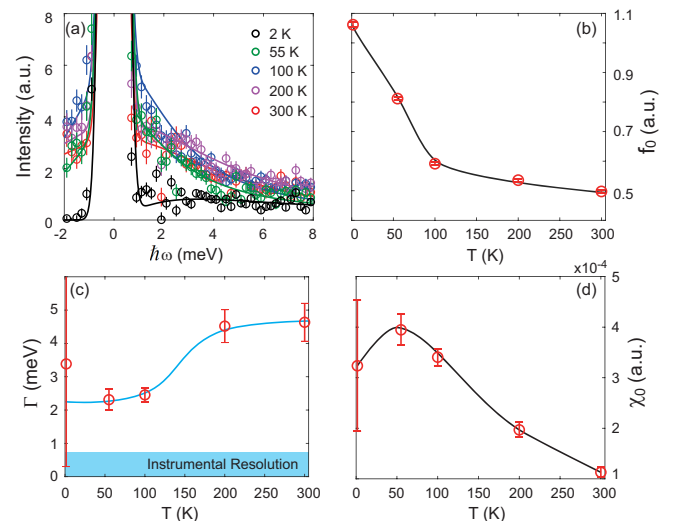

FIG. 4. (a) Constant-$\boldsymbol{Q}$ energy spectra of neutron scattering intensities at five different temperatures. The solid lines are results from our fitting. (b)–(d) The estimated f_0, line widths of the Lorentzian function, Γ, and the staggered susceptibility, $\chi_0(\boldsymbol{Q})$ at $\boldsymbol{Q} = (0.5, 1.5, 0)$, as a function of temperature. The blue shaded area represents the instrumental resolution.
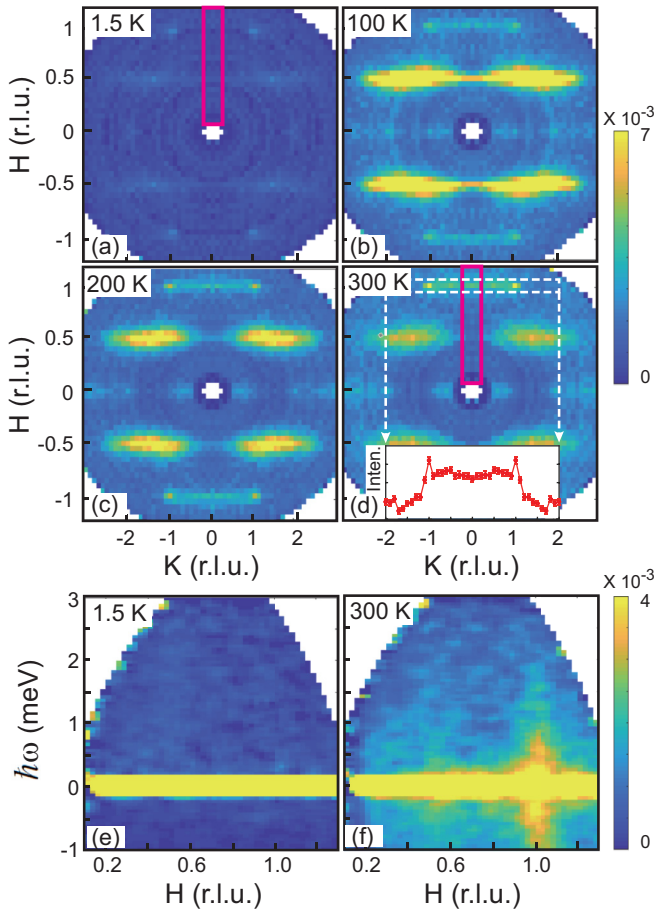
FIG. 5. (a)–(d) Inelastic neutron scattering intensities integrated in the $\hbar\omega$ range of 0.3–0.7 meV in the [H, K, 0] plane at four different temperatures. Inset in (d) shows a one-dimensional (1D) cut along [1, K, 0] in the area enclosed by a white dashed rectangle. (e) and (f) Slices of intensities along the direction as marked by the pink rectangles in (a) and (d) as a function of H and energy at the base temperature and 300 K, respectively.

tures. These maps are at energies smaller than the data shown in Fig. 2, well within the quasi-elastic peak but outside the elastic resolution. In addition to the strong AFM spin fluctuations at half-integer H discussed above, we clearly see additional excitations with prolate profiles like the surfboard correlations along the K direction but at integer H, such as at $\boldsymbol{Q} = (1, 0, 0)$. An example of the K dependence of these excitations is shown for $H = 1$ in the inset of Fig. 5(d). The two sharp peaks centered at $K = -1$ and 1 are due to acoustic phonons emanating from the $\boldsymbol{Q} = (1, -1, 0)$ and (1,1,0) Bragg peaks, but the additional broad peak is centered at $\boldsymbol{Q} = (1, 0, 0)$, which is a forbidden wave vector for structural Bragg peaks in the $Cmcm$ space group and is therefore not due to acoustic phonons. Furthermore, as seen in Fig. 5(f), these excitations are only observable below $\hbar\omega = 2$ meV and exhibit the highest intensities at the highest measured temperature (300 K) [Fig. 5(d)], in contrast to the fluctuations at half-integer H which are maximal close to T_g and are strongly suppressed at base temperature [Fig. 5(e)]. Note that, if spins point along $\boldsymbol{a}$, as was modeled in our previous work [24], magnetic intensity is forbidden at $\boldsymbol{Q} = (1, 0, 0)$
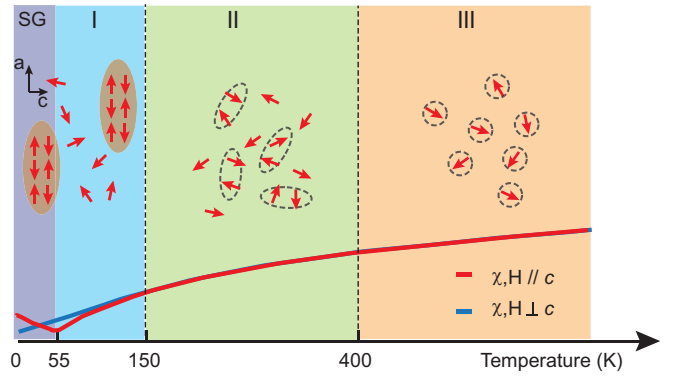

FIG. 6. A combined phase diagram determined by magnetic susceptibility and neutron scattering. At high temperatures > 400 K, isolated magnetic moments are not correlated, and the susceptibility follows the Curie-Weiss law. Between 150 and 400 K, the deviation from Curie-Weiss law reflects the presence of correlation between magnetic moments. Below 150 K, the surfboard structure is formed, and the anisotropy between a and c axes start to develop. Below $T_g \sim 55$ K, the dynamic surfboard is frozen and becomes static, while the surrounding spin clouds are still dynamically fluctuating.

because neutrons are only sensitive to the component of spin perpendicular to $\boldsymbol{Q}$. While clearly visible here in the inelastic channel, these additional maxima centered at integer H are very weak and due to other, stronger scattering contributions in the elastic channel [see Fig. 5(f)] had not been noticed in the previous work and are also not observable here when the data are integrated over $\hbar\omega = 0$. Nevertheless, it can be insightful to consider the structure factor based on the previously proposed surfboard model but with the addition of a c-axis canting within the surfboard. We found that this canting would indeed lead to broad maxima centered at integer H, including $\boldsymbol{Q} = (1, 0, 0)$. Thus, a possible interpretation of the present observation is that the diffuse streaks observed at integer H arise from fluctuating surfboard spins that have instantaneous correlations with a small canted component along c. Let us note that, while the a-axis moments are still completely frustrated between neighboring double spin chains as proposed previously, the presence of c-axis canting moments could slightly relax the frustration to a certain extent that the correlation length along the b axis is not perceivably affected.

IV. SUMMARY

It is useful to summarize pictorially the present results of the temperature dependence of the spin correlations with reference to the pseudophase diagram presented in Ref. [24]. At elevated temperatures (region III in Fig. 6), the magnetic susceptibility is Curie-Weiss-like and isotropic, reflecting paramagnetic behavior of spins which have instantaneous nearest-neighbor AFM correlations but with no extended, surfboard correlations. We surmise that the appearance of fluctuating intrasurfboard correlations coincides with the deviation from the Curie-Weiss law < 400 K in Region II. It is worth mentioning that the extra spin fluctuations at $\boldsymbol{Q} = (1, 0, 0)$ also appear in this temperature range. Here, the intrasurfboard correlations are fluctuating, and they slow as

the temperature is lowered and the relaxation rate decreases. The susceptibility shows no appreciable anisotropy in Region II. However, <150 K, the system enters Region I, where the dynamics of intrasurfboard correlations have appreciably slowed down and anisotropy appears in the susceptibility. At T_g, the spectral weight of intrasurfboard correlations is rapidly increasing in the elastic channel, and the fluctuating susceptibility has peaked. If we consider the anisotropic peak in susceptibility at T_g to be a consequence of intersurfboard interactions, the implication here is that the freezing of the intersurfboard dynamics is strongly correlated to the freezing of the intrasurfboard dynamics. Nevertheless, well below T_g,

some intrasurfboard fluctuations remain, as is also indicated by the anisotropic susceptibility [24].

[1] K. Binder and A. P. Young, Rev. Mod. Phys. **58**, 801 (1986).

[2] I. Klich, S.-H. Lee, and K. Lida, Nat. Commun. **5**, 3497 (2014).

[3] J. Yang, A. Samarakoon, S. Dissanayake, H. Ueda, I. Klich, K. Lida, D. Pajerowski, N. P. Butch, Q. Huang, J. R. D. Copley *et al.*, Proc. Natl. Acad. Sci. USA **112**, 11519 (2015).

[4] L. Balents, Nature (London) **464**, 199 (2010).

[5] J. S. Gardner, M. J. P. Gingras, and J. E. Greedan, Rev. Mod. Phys. **82**, 53 (2010).

[6] S. V. Syranov and A. P. Ramirez, Nat. Commun. **13**, 2993 (2022).

[7] S. Shtrikman and E. P. Wohlfarth, Phys. Lett. A **85**, 467 (1981).

[8] C. Pappas, F. Mezei, G. Ehlers, P. Manuel, and I. A. Campbell, Phys. Rev. B **68**, 054431 (2003).

[9] A. P. Murani, J. Appl. Phys. **49**, 1604 (1978).

[10] A. P. Murani and J. L. Tholence, Solid State Commun. **22**, 25 (1977).

[11] B. Hennion, M. Hennion, F. Hippert, and A. P. Murani, J. Phys. F: Met. Phys. **14**, 489 (1984).

[12] K. Motoya, T. Freltoft, P. Boni, and G. Shirane, Phys. Rev. B **38**, 4796 (1988).

[13] J. S. Gardner, B. D. Gaulin, S.-H. Lee, C. Broholm, N. P. Raju, and J. E. Greedan, Phys. Rev. Lett. **83**, 211 (1999).

[14] J. C. Gómez Sal, J. García Soldevilla, J. A. Blanco, J. I. Espeso, J. Rodríguez-Fernández, F. Luis, F. Bartolomé, and J. Bartolomé, Phys. Rev. B **56**, 11741 (1997).

[15] R. S. Solanki, S.-H. Hsieh, C. H. Du, G. Deng, C. W. Wang, J. S. Gardner, H. Tonomoto, T. Kimura, and W. F. Pong, Phys. Rev. B **95**, 024425 (2017).

[16] X. Lu, D. W. Tam, C. Zhang, H. Luo, M. Wang, R. Zhang, L. W. Harriger, T. Keller, B. Keimer, L.-P. Regnault *et al.*, Phys. Rev. B **90**, 024509 (2014).

[17] U. Atzmony, E. Gurewitz, M. Melamud, H. Pinto, H. Shaked, G. Gorodetsky, E. Hermon, R. M. Hornreich, S. Shtrikman, and B. Wanklyn, Phys. Rev. Lett. **43**, 782 (1979).

[18] Y. Yeshurun, I. Felner, and B. Wanklyn, Phys. Rev. Lett. **53**, 620 (1984).

[19] Y. Yeshurun and H. Sompolinsky, Phys. Rev. B **31**, 3191 (1985).

[20] J. K. Srivastava, W. Treutmann, and E. Untersteller, Phys. Rev. B **68**, 144404 (2003).

[21] J. Rodrigues, W. S. Rosa, M. M. Ferrer, T. R. Cunha, M. J. M. Zapata, J. R. Sambrano, J. L. Martinez, P. S. Pizani, J. A. Alonso, A. C. Hernandes *et al.*, J. Alloys Compd. **799**, 563 (2019).

[22] Y. Yeshurun, J. L. Tholence, J. K. Kjems, and B. Wanklyn, J. Phys. C: Solid State Phys. **18**, L483 (1985).

[23] R. L. Lichti, S. Kumar, and C. Boekema, J. Appl. Phys. **63**, 4351 (1988).

[24] P. G. LaBarre, D. Phelan, Y. Xin, F. Ye, T. Besara, T. Siegrist, S. V. Syzranov, S. Rosenkranz, and A. P. Ramirez, Phys. Rev. B **103**, L220404 (2021).

[25] F. Ye, Y. H. Liu, R. Whitfield, R. Osborn, and S. Rosenkranz, J. Appl. Cryst. **51**, 315 (2018).

[26] P. Miao, R. Wang, W. Zhu, J. Liu, T. Liu, J. Hu, S. Li, Z. Tan, A. Koda, F. Zhu *et al.*, Appl. Phys. Lett. **114**, 203901 (2019).

[27] G. Ehlers, A. A. Podlesnyak, and A. I. Kolesnikov, Rev. Sci. Instrum. **87**, 093902 (2016).

[28] O. Arnold, J. C. Bilheux, J. M. Borreguero, A. Buts, S. I. Campbell, L. Chapon, M. Doucet, N. Draper, R. Ferraz Leal, M. A. Gigg *et al.*, Nucl. Instrum. **764**, 156 (2014).

[29] These values were obtained by fitting the elastic line with a Gaussian function and agree with the estimation from the Py-Chop model, https://rez.mcvine.ornl.gov/.